First-principles theoretical investigation of monoatomic and dimer Mn adsorption on noble metal (111) surfaces

Francisco Muñoz,[1,2] Aldo H. Romero,[3] Jose Mejía-López,[2,4] and J. L. Morán-López[5]

[1]*Departamento de Física, Facultad de Ciencias, Universidad de Chile, Casilla 653, Santiago, Chile*

[2]*Centro para el Desarrollo de la Nanociencia y la Nanotecnología CEDENNA, Avenida Ecuador 3493, Santiago, Chile*

[3]*CINVESTAV, Unidad Querétaro, Libramiento Norponiente 2000, Real de Juriquilla, CP 76230, Querétaro, México*

[4]*Facultad de Física, Pontificia Universidad Católica de Chile, Casilla 306, Santiago, Chile*

[5]*Departamento de Física, Laboratorio Interdisciplinario, Facultad de Ciencias, Universidad Nacional Autónoma de México, México Distrito Federal, México*

(Received 7 July 2011; published 12 March 2012)

A theoretical investigation of the adsorption of Mn single atoms and dimers on the (111) surface of Cu, Ag, and Au, within the framework of the density functional theory, is presented. First, the bulk and the clean (111) surface electronic structures are calculated, with results that agree well with previous reports. To understand the adatom-substrate interaction, also the electronic characteristics of the free Mn dimer are determined. Then, the electronic structure of the Mn adatom, chemisorbed on four different surface geometries, is analyzed for the three noble metals. It is found that the most stable geometry, in all three cases, Cu, Ag, and Au, occurs when the Mn atom is chemisorbed on threefold coordinated sites. For the dimer, the lowest-energy configuration corresponds to the molecule lying parallel to the surface. In the three noble metals, the geometry corresponds to both atoms chemisorbed in threefold coordinated sites, but with different local symmetry. It is also found that the magnetic configuration with the lowest energy corresponds to the antiferromagnetic arrangement of Mn atoms, with individual magnetic moments close to $5\mu_B$. The ferromagnetic and antiferromagnetic solutions, in the case of a Ag substrate, are close in energy. It is also found that in this case the Mn_2 molecule is chemisorbed with very similar energy on various geometries. To study the dynamical motion of the dimer components, we calculated the potential energy barriers for the Mn motion in the various surfaces. In contrast to Cu and Au, this leads to the conclusion that on Ag the Mn dimer moves relatively freely.

DOI: 10.1103/PhysRevB.85.115417 PACS number(s): 68.43.−h

I. INTRODUCTION

The impressive development of experimental techniques to synthesize, characterize, and design special nanostructures with specific size and composition[1] has opened a very attractive field of research to determine and understand their unexpected physicochemical properties. These methods include the deposition and manipulation of single atoms, small clusters, and monolayers on metal surfaces. Due to the potential technological applications in ultrahigh-density data storage and spin injection devices, particular interest has been attracted to the study of magnetic nanostructures. Among them, the growth of ultrathin films or nanostructures, based on magnetic transition metals and deposited on various substrates, has been the subject of very intense research.[2–7] More recently, it has also been revealed that adatoms or small magnetic nanostructures can interact through long-range interactions mediated by the metallic substrate: a Ruthermann-Kittel-Kasuda-Yoshida kind of interaction.[8,9] That interaction may be more important than the direct exchange interaction for distant chemisorbed atoms.

In recent decades, due to the fact that Mn is the transition metal with the highest atomic magnetic moment ($5\mu_B$), much attention has been paid to the deposition of Mn nanostructures on metallic substrates. An overlayer of ferromagnetically (FM) coupled atoms, with such a high magnetic moment, would be an excellent candidate for technological applications, for example in spintronics.[10] However, in order to be subject to applications, magnetic nanostructures must be stable for an extended time, at high temperatures. Thus, a large magnetic anisotropy energy is needed; a characteristic difficult to obtain in systems with a small spin-orbit interaction.

However, Mn by itself is a very intriguing element. It is well known that Mn, in bulk samples, presents a rich variety of magnetic behaviors, depending on crystalline structure, temperature, and pressure.[11] A complex behavior is also observed in small clusters, where the average magnetic moment (μ_{ave}) shows a nonmononotonous size dependence.[12] It is then expected that Mn low-dimensional chemisorbed systems would also show a diversity of magnetic characteristics.

The size dependence of μ_{ave} was analyzed theoretically by Mejía *et al.*,[13] who arrived at the conclusion that, due to antiferromagnetic (AFM) interactions between nearest neighbors and ferromagnetic coupling among more distant pairs, complex noncollinear structures are produced. These calculations on free Mn dimers showed that the magnetic lowest-energy state depends on the distance between the two atoms.[13,14] The ferromagnetic and antiferromagnetic configurations are stable above and below 3.06 Å, respectively. However, they found that the ground state of the free dimer is the antiferromagnetic arrangement with a bond distance of 2.89 Å. Thus, it is interesting to investigate if the chemisorption of Mn on particular substrates and surface orientations forces the Mn-Mn nearest-neighbor bond length to generate a ferro- or antiferromagnetic coupling and produce, for high coverages, the appearance of magnetic phases. This is the case of the antiferromagnetically ordered monolayer of Mn atoms chemisorbed on the Ag(001) surface.[15] In that study, it was also found that the epitaxial growth of Mn single-crystal films exhibits a tetragonal rather than cubic structure.

Furthermore, it has been observed that the growth of Mn on noble metal substrates, in general, evolves in the following way: for low coverage the adatoms remain at the surface on particular sites. Upon increasing the coverage, there is a tendency to exchange sites between the top-most surface atoms and Mn, forming Mn monolayers intercalated with the metallic substrate. Further deposition leads to Mn islands. This growth mechanism has been observed, by scanning tunneling microscopy and other techniques, in Cu(100),[16] Cu(110),[17] Ag(100),[18] and Au(111).[19]

For applications, the most interesting case is when the Mn atoms form a monolayer at the metal surface. Wuttig *et al.*[20] reported the monolayer growth of Mn on Cu(100), and they claimed that the stability of this structure is produced by the Mn magnetic properties. They also estimated a Mn magnetic moment of $3.64\mu_B$. More recently, a ferromagnetic order has been observed through x-ray magnetic circular dichroism.[21] However, the researchers estimate a very small magnetic moment ($0.67\mu_B$). There is also a report on the chemisorption of Mn on Cu(110), but no conclusive results with respect to the magnetic properties were obtained.[22]

In the case of a gold substrate, the growth mechanism of manganese on the (111) surface has been reported.[19] In the submonolayer regime a Mn-Au alloy was observed to form. Between this deposited amount and three monolayers, a layer-by-layer growth of fcc Mn film is obtained. Further deposition leads to the cubic bulk structure. This report does not contain magnetic studies.

In addition to the experimental reports, a more fundamental motivation to study Mn on noble metals is to understand the interplay between the different orbitals on the bonding process to metallic substrates. In general, it is expected that adsorption decreases the atomic magnetic moment due to the electronic hybridization with the surface atoms, unless a charge transfer from the surface to the majority spin levels compensates for that reduction.

Another important theoretical aspect is that in small clusters the state of lowest energy occurs when the atomic magnetic moments do not orient collinearly. This result has been reported in several *ab initio* and semiempirical calculations in both supported[23] and free-standing Mn clusters.[13,24] Now, there is a general consensus that Mn clusters supported on a metal surface develop noncollinear ordering due *mainly* to frustration in the AFM order.[25] Another feature observed in small deposited or free Mn clusters is that the magnetic bistability, i.e., the energy of FM and AFM ordered structures, is almost degenerate,[26] and both states may coexist. Finally, it is important to note that most theoretical studies of Mn clusters supported on noble metals neglect a proper structural optimization of the substrate, mainly due to a high computational cost. Nevertheless, we are convinced that a clear interpretation of the chemisorption process of a simple adatom or of dimer molecules, including the structure optimization, is of vital importance to understand the growth and properties of larger nanostructures.

Here, we report a set of total energy calculations of the adsorption of Mn single atoms and dimers on Cu, Ag, and Au (111) surfaces. We calculate the electron density distribution, the magnetic moment, and the bond lengths with Mn chemisorbed on various geometrical sites. The results for the Au(111) surface were reported recently,[27] which we include here for comparison with silver and copper. To study the stability of the chemisorbed dimers, we calculated the potential energy barriers to move one Mn atom along various paths. We found that for Cu and Au it is difficult to brake the dimer once it is stabilized at the surface. A different behavior is observed in the Ag surface, where the barriers to move the Mn atoms to neighbor sites are almost negligible. This leads us to conclude that Mn atoms can exchange sites very easily and the dimer diffusion can be observed at room temperature. We should also point out that, since we are considering a slab of five layers (a restriction imposed by the computation complexity), our results of the surface electronic states may not reflect some features of the real semi-infinite system.[28,29] Obviously, our model can be improved as the number of layers can be increased.

In Sec. II a brief description of the computational approach is presented. Then, in Sec. III, we discuss the clean noble metal (111) surface properties and compare our findings with previous results reported in the literature. The energetics and structure of a single Mn atom adsorption on that surface are presented in Sec. IV. The results on the adsorption of the Mn dimer are contained in Sec. V. The diffusion barriers for Mn motion are calculated and discussed in Sec. VI. Finally, we discuss our results and present the conclusions in Sec. VII.

II. COMPUTATIONAL METHODS

Our calculation is based on the density functional theory (DFT)[30] as implemented within the framework of the Vienna *Ab initio* Simulation Package (VASP) code.[31–34] We consider only valence electrons and describe them with projector-augmented-wave (PAW) type pseudopotentials,[35,36] which allows us to take into account spin-orbit interactions (SOIs). As mentioned in a previous paper,[27] although the SOIs are stronger in Au than in Ag and Cu, and stronger even than in Mn, it is not relevant to take them into account in the study of Mn chemisorption (basically, SOIs change the total energy but energy adsorption is obtained after substraction, which reduces the spin-orbit effect). For the exchange correlation we use the Perdew-Burke-Erhenzof (PBE) description.[37] The energy cutoff for the plane waves was set at 260 eV in all calculations. This value assures a force convergence of less than 0.01 eV/Å.

To test the exactness of the approximations made, we calculated first the ground-state structure of the bulk noble metals. We found that all of them adopt a fcc geometry with lattice parameters of 3.59, 4.00, and 4.17 Å for Cu, Ag, and Au, respectively. Those values compare well with the reported experimental values: 3.61, 4.09, and 4.08 Å.[38] We also found that the calculated electronic structure reproduces very well the results from previous reports. With the confidence that our approximation describes to a good accuracy the bulk system, we calculated next the electronic structure of the metallic (111) surfaces. We modeled the surface region by a slab of five layers; two of them were kept fixed to the bulk parameters and the other three were allowed to relax. We found that the distance between the surface layer and the second layer, d_{12}, contracts by -1.2% (-0.7%),[39] -4.9% (-2.5%)[40] for Cu and Ag, and expands by 2.0% (3.3%)[41] in the Au case. The experimental

values are given inside the parentheses, showing an acceptable agreement.

To study the Mn adsorption, we employed a 3×3 supercell (1/9 coverage) along the surface plane and considered the five layers modeling the substrate. Due to the fact that the wave function is expanded in plane waves, we have to consider a large empty space between periodic images perpendicular to the surface. In our calculation we took the value of 12 Å (equivalent to approximately five surface layers). We checked that our results do not depend on this specific value. The surface energy changes by less than 0.01% when this distance is increased to 14 Å. Furthermore, in the calculation of the surface electronic structure and the adsorption process, the geometry was relaxed until the forces were smaller than 0.03 eV/Å. Finally, due to the metallic character of the surface, we considered a K mesh of $12 \times 12 \times 1$, which guarantees an accuracy of 0.01 eV in the total energy of the 3×3 supercell.

III. NOBLE METAL CLEAN SURFACE

We calculated the electronic structure of several relaxed (111) noble metal surfaces (Au, Cu, and Ag). We allowed the condition that the surface atoms relax in all directions. However, as expected, the most important changes are in the direction perpendicular to the surface. We present in Fig. 1 the electronic redistribution that takes place at the atoms close to the surface. We plot the difference between the converged charge density of the semi-infinite system $\rho_{\text{semi-inf}}$ and the charge density of the free atomic charge densities ρ_{atomic} located at the equilibrium sites,

$$\delta\rho = \rho_{\text{semi-inf}} - \rho_{\text{atomic}}. \tag{1}$$

This function helps one to see the electronic rearrangement produced by the solid bonding, and it reflects the local symmetry of the surface atoms. The upper, middle, and lower sets of figures corresponds to Cu, Ag, and Au, respectively. In the left panel, we show the atoms at the surface layer. The color scale is given on the right-hand side. Positive values (light yellow) mean a higher electron density in the composed system as compared to the atomic distribution, and negative values (black in Cu, red in Ag and Au) denote zones where the opposite occurs. It is remarkable that in the Cu atoms there is a larger rearrangement of charge compared to Ag and Au. This effect has its roots in both the smaller charge at the nucleus and the shorter interatomic distance (∼14%) in the solid compared to the other two noble metals.

In the three right panels, we show the charge distribution on planes perpendicular to the surface and passing through the various stacking lines of atoms. The first one shows the side view of the electronic distribution on the plane that passes through the surface atoms (type A), and those on the fourth layer. One sees that the surface atoms resemble more the atomic electron configuration, due to the smaller coordination and the metallic character. The next panel shows the distribution on a plane that passes through the atoms at the second and fifth stacking layers (type B). One can notice in Au a slight effect produced by the surface, while for the other metals it is hard to see any surface effect in this layer. The right-most panel corresponds to the electronic distribution on a plane passing through the third layer, corresponding to atoms in the fcc stacking sequence of type C. One does not see any surface effect in this plane. This result is also driven by the fact that the fourth and fifth layers are set to the bulk parameters.

The relaxation procedure produces different effects: we obtained a small contraction in Cu and Ag ($d_{12} = -1.2\%$, -4.9%, respectively), while in Au we found an expansion of the distance between the surface and second layer, $d_{12} = 2\%$. It is worth noticing that, for the former metals, which show a contraction, the electronic cloud of the relaxed surface shows a stronger interaction among the first and second layer atoms (the high negative values for $\delta\rho$ close to the atoms reflect this fact), while for Au the expansion reduces further the low coordination of the outermost layer, which also reduces the interaction among atoms and makes the electronic cloud more localized close to the ions (see Fig. 1).

Experimentally, it has been observed by a refined low-energy electron diffraction (LEED) study[39] that the distance between the two top layers of the (111) Cu surface contracts by $-0.7 \pm 0.5\%$. In the case of the (111) Ag surface, it has been reported using the medium-energy ion scattering technique[40] that the distance d_{12} contracts by -2.5% at room temperatures. This situation changes as a function of temperature and expands by about 10%, 80 K before the melting point. Finally, the (111) Au surface was studied by x-ray scattering,[41] and a 3% expansion was reported. Thus, our calculations of the three noble metal (111) surfaces reproduce well the experimental observations.

We calculated the surface energy, as defined by the equation

$$E_s = \frac{E_{\text{semi-inf}} - N E_{\text{bulk}}}{2N}, \tag{2}$$

where E_{bulk} is the energy per atom in the bulk, $E_{\text{semi-inf}}$ is the energy of the semi-infinite system, and N is the number of surface atoms involved. Our numerical results are given in Table I. Here, we compare our results with previous theoretical studies, based on two different methods.[42,43]

The noble metal (111) surfaces are stable with regard to reconstruction, with the exception of gold. In this last case, the reconstruction consists of the periodic displacement of 46 surface atoms (two rows of 23), where close to 2/3 are in a fcc arrangement and around 1/3 are in hcp locations. It has been shown that, to simulate the experimental reconstruction of the Au(111) surface, it is necessary to consider a very large $(22 \times \sqrt{3})$ cell,[44] which demands important computational resources. Nevertheless, this effect does not influence our chemisorption calculation, since our cell is much smaller than the one needed to model the reconstruction. Thus, for our purposes we do not need to take into account the reconstruction phenomena. Furthermore, it has been shown that the chemical activity of the surface is dominated by the top-most surface atoms that follow the fcc stacking.[44]

Taking into account the spin-orbit interactions (SOIs) in the noble metal substrate atoms, the surface energy increases by 36%, 1.5%, and 1% in the cases of Au, Ag, and Cu, respectively. However, the effects in the geometrical structure are negligible, since the interatomic distances change only by approximately 0.01 Å. Thus we ignore this kind of interaction in the rest of this report.

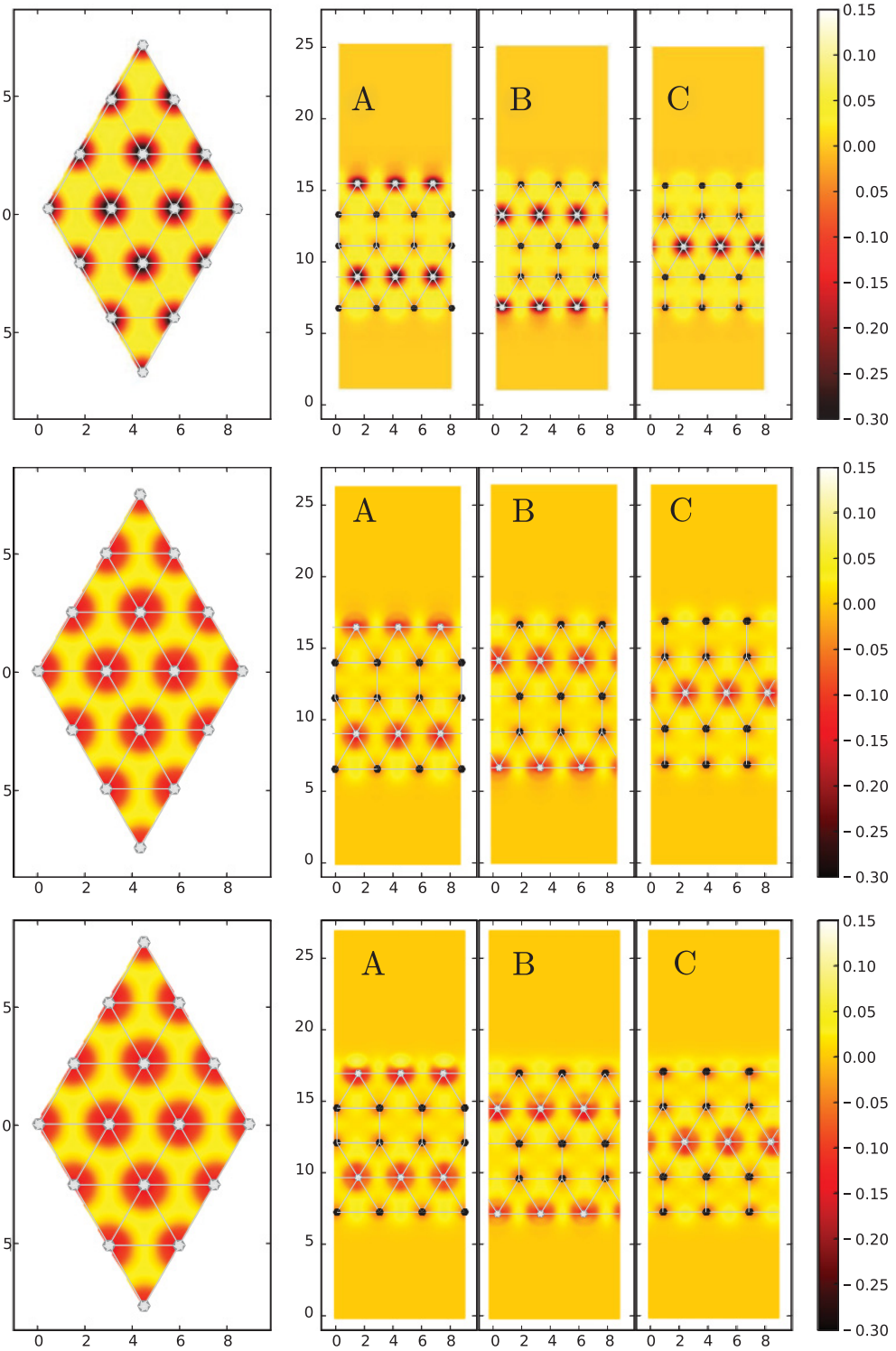

FIG. 1. (Color online) Electronic charge redistribution $\delta\rho$ of the atoms at the (111) relaxed surface. The upper, middle, and lower panels correspond to the Cu, Ag, and Au surfaces, respectively. The left images show the top-most surface plane passing through the relaxed surface atoms. The images A, B, and C show the electronic redistribution at planes perpendicular to the surface and passing through the atoms of the three different layers (ABC fcc stacking). In particular, the small linked circles show the atoms at the relaxed surface. The distances are in Å, and the color bars are in $e/\text{Å}^3$.

IV. SINGLE Mn ATOM ADSORPTION

We proceed now with the adsorption of a single Mn atom. As shown in Fig. 2, the (111) fcc surface offers four different symmetric adsorption sites: on top of a surface atom (A), in the bridge position between two surface atoms (AA), or in threefold coordinated sites. The threefold coordinated sites

TABLE I. Calculated surface energy (E_s) in eV/Å^2, compared to published results.

E_s	Cu	Ag	Au
This work	0.086	0.033	0.044
Ref. 42	0.088	0.068	0.055
Ref. 43	0.073	0.038	0.049

are of two types: one that follows the hcp sequence (B) and another that follows the fcc stacking order (C). In Fig. 2, the purple circles A, B, C, and AA denote the chemisorption sites, and the dark, gray, and light circles denote the first, second, and third layer surface atoms.

We performed an unconstrained optimization of the geometry of the adatom and the three surface layers by keeping fixed the two deeper layers to mimic the bulk. In this calculation we allowed also the relaxation of the spin degrees of freedom.

In Table II we present the results for the adsorption energy, at the three noble metal surfaces, defined as follows:

$$E_A = \frac{E_{\text{Total}} - E_{\text{semi-inf}} - NE_{\text{Mn}}}{N}, \quad (3)$$

where E_{Total} is the energy of the chemisorbed atom on the surface, $E_{\text{semi-inf}}$ is the energy of the semi-infinite system, and N is the number of adsorbed Mn atoms, for each of the nonequivalent adsorption sites. In this table we also give the results for the distance between the Mn atom and the surface plane, $d_{\text{Mn-surf}}$, in Å.

We find that the highest adsorption energies for Cu, Ag, and Au are 2.48, 1.96, and 2.81 eV, respectively. Those are the energies when the Mn atom is chemisorbed on threefold coordinated sites; B for Cu and Ag, and C for Au. It is important to notice that, in the case of Cu, we obtain the same energy when Mn is chemisorbed on B or C sites. On the other hand, the chemisorption energies on twofold coordinated sites AA also share the ground state for Cu, and are very close in energy to the three coordinated sites in the Ag surface. That is not the case for Au, where the energy at the bridge site is clearly smaller. The similarity of energies obtained for the threefold and twofold

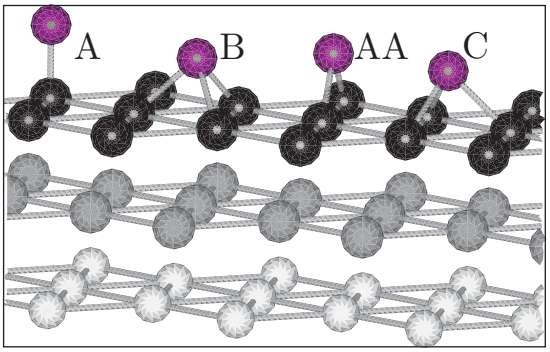

FIG. 2. (Color online) Adsorption sites on a fcc (111) surface. The site of type A is on the top of a surface atom, B and C are above the surface and coordinated to three surface atoms, and AA is bonded to two surface atoms. The difference between B and C is that B has a noble metal neighbor in the second layer while C does not. The dark, gray, and light circles denote the first, second, and third layer surface atoms.

TABLE II. The adsorption energy in eV, the Mn magnetic moment in μ_B, and the distance between the Mn atom and the surface plane ($d_{\text{Mn-surf}}$) in Å, for the different chemisorption sites at the surface of Cu, Ag, and Au.

	E_A			μ			$d_{\text{Mn-surf}}$		
Site	Cu	Ag	Au	Cu	Ag	Au	Cu	Ag	Au
A	−2.18	−1.68	−1.95	4.60	4.82	5.07	2.26	2.48	2.44
B	−2.48	−1.96	−2.80	4.53	4.72	4.83	2.48	2.66	2.58
C	−2.48	−1.94	−2.81	4.53	4.77	4.82	2.46	2.69	2.58
AA	−2.48	−1.94	−2.73	4.52	4.75	4.83	2.40	2.61	2.52

coordinated sites is due to the fact that the site AA is bonded to two nearest neighbors and two next-nearest neighbor atoms at the surface layer. The distance at which nearest and next-nearest neighbors are located differs only by a small amount, i.e., they are 17%, 14%, and 17% larger for Au, Ag, and Cu, respectively. Thus, the bridge site is competitive with respect to B and C, which indicates that in the growing process, due to its dynamical dependence, the adsorption on B, C, and AA will depend mostly on the relative numbers of those sites. The adsorption in an A site produces a large electronic localization around the Mn atom, which probably is responsible for the weakest bonding energy among all the considered sites. From these results we conclude that the adsorption of Mn clusters on noble metal surfaces is ruled by the Mn-surface interaction, since the bonding energies are at least four times larger than the Mn-Mn free-dimer bonding energy (around 0.53 eV).

We also find that the distance from the adatom to its closest surface neighbor, when chemisorbed on B or C sites, is nearly the same, but different for each surface. On the other hand, the distance $d_{\text{Mn-surf}}$ in AA sites is $\sim$2.5% shorter than the respective B or C distances for each element. As expected, the shortest chemisorption distance corresponds to the A sites.

In Table II, we also give the results for the Mn atomic magnetic moment μ, in Bohr magnetons (μ_B). We notice that μ is very similar in B, C, and AA sites: $\sim 4.5\mu_B$, $\sim 4.7\mu_B$, and $\sim 4.8\mu_B$ for Au, Ag, and Cu, respectively. The highest values correspond to Mn chemisorbed on A sites and are $4.6\mu_B$, $4.82\mu_B$, and $5.07\mu_B$ for Cu, Ag and Au, respectively.

To better understand the adsorption on the various sites at an electronic level, one can plot the difference $\delta\rho$ between the converged charge density of the surface with the Mn atom and the superposition of the free atomic charge densities. From Fig. 3 one can see marked differences between the adsorption over an A site and the adsorption at other sites: the A-site adsorption affects more significantly the substrate atom below, and pushes it inside the solid. One notices also that some electrons are pulled from the surface neighbors and accumulated, mainly close to the Mn and the surface atom below. There is also a small accumulation of electronic charge on the surface neighbors (Mn losses are of the order of $\frac{1}{4}e^-$ after adsorption, mostly from s-like orbitals).

In the cases B, C, and AA, the charge redistributions are very similar, giving rise to small differences. In these cases the bonding is more uniform: the Mn not only shares its electrons with its nearest substrate atoms, but also does so with the metallic surface electronic cloud. This fact makes E_A (around

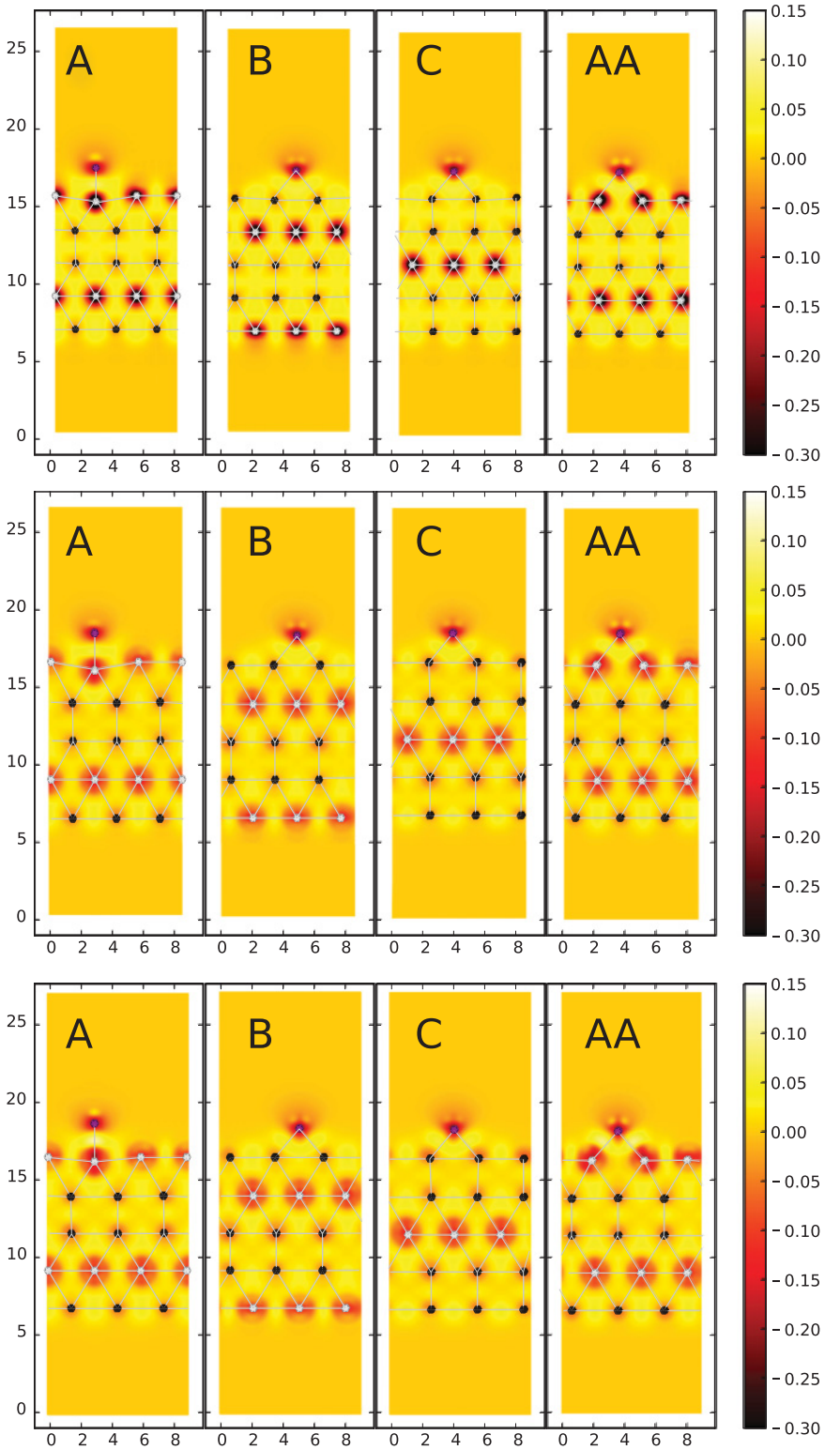

FIG. 3. (Color online) Charge redistribution $\delta\rho$ for each adsorption site of a (111) noble metal surface. The upper, middle, and lower panels are respectively for Cu, Ag, and Au substrates. The red circles denote the Mn and the substrate atoms located at the same plane. The distances are in Å, and the color bars are in $e/\text{Å}^3$.

0.3 eV for Cu and Ag, and 0.9 eV for Au) larger than in the chemisorption on an A site. One also observes that the electronic rearrangements due to the adatom have little effect deeper than the second substrate atomic layer.

Figure 4 shows the local electronic density of states (LDOS) of Mn (red line) at each adsorption site and the corresponding average LDOS of the neighbor atoms on the (111) noble metal surface (black line). In each panel we show in the upper (lower) part the up $\rho_\uparrow(E)$ [down $\rho_\downarrow(E)$] spin states. The Fermi energy (E_F) corresponds to the zero in the energy scale and the magnetic moment is calculated by

$$\mu = \int_{-\infty}^{E_F} [\rho_\uparrow(E) - \rho_\downarrow(E)] dE. \quad (4)$$

Despite the fact that the three substrates have the same valence, the interaction between the Mn states and the substrate atoms

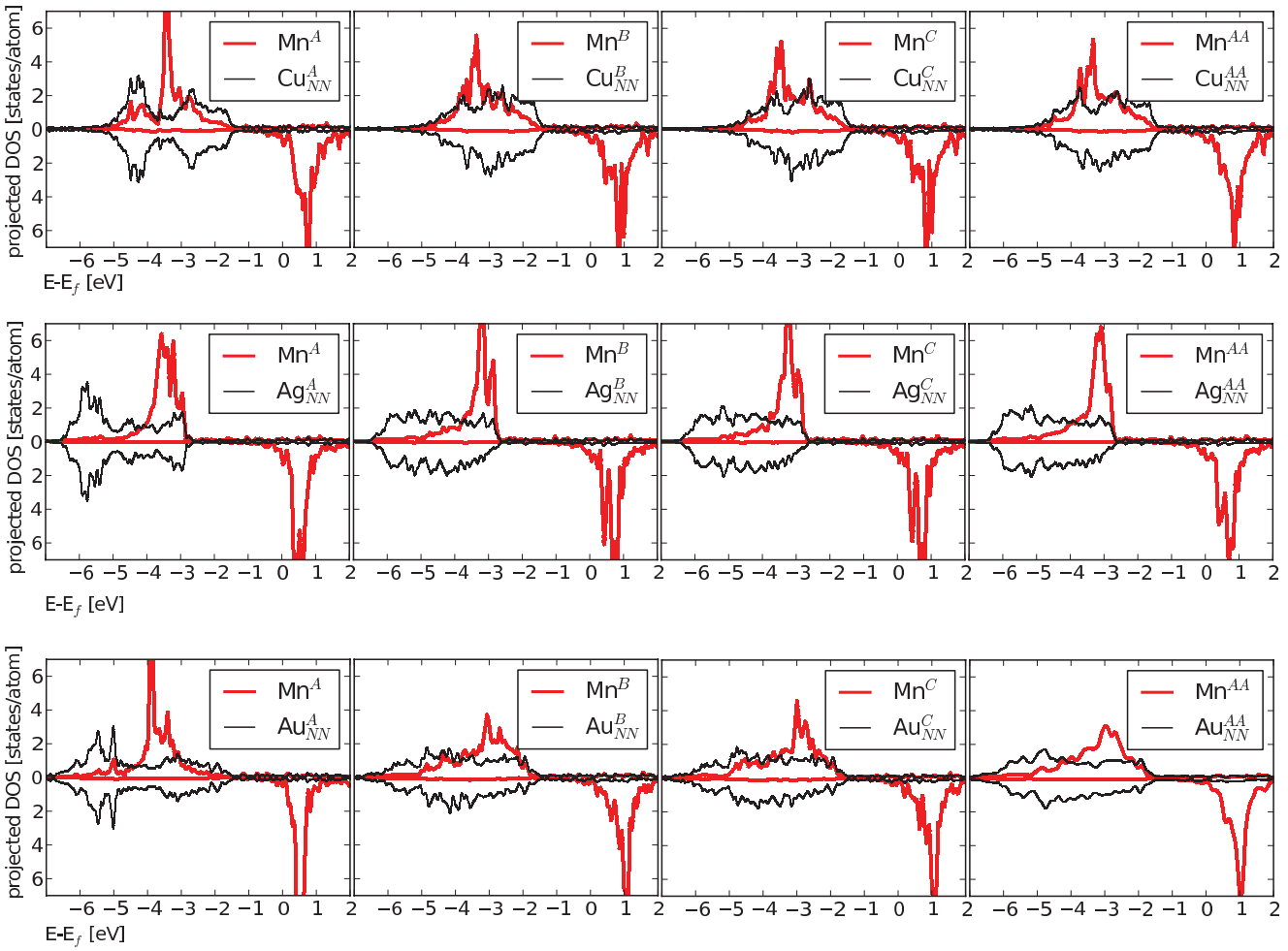

FIG. 4. (Color online) Local electronic density of states (LDOS) on Mn (red lines) and on the nearest-neighbor (111) surface atoms (black lines). Each adsorption site is indicated as a superscript in the chemical symbols. M_{NN} is the DOS of the nearest-neighbor surface atom M (where M is Cu, Ag, and Au for the upper, middle, and lower panels). In each panel, the upper (lower) part corresponds to up (down) spin electrons.

depends on their relative position. The LDOS of surface nearest-neighbor substrate atoms reflects the presence of the Mn atom. In the A case, the surface LDOS presents, in the low-energy part, peaks produced by the interaction with the Mn atom chemisorbed on the top. The cases B and C show wider bands and there are only very slight differences. A more continuous density of states is obtained in the AA case, due to the higher effective coordination number. The highest magnetic moment in the state with lowest energy occurs for Au ($4.82\mu_B$), when the Mn atom is chemisorbed in a C site. In the substrate atoms, we notice a rather small asymmetry between up and down states, a fact that produces only small magnetic moments ($\approx 0.05\mu_B$ in the nearest Mn neighbors, and one order of magnitude smaller on the second neighbors).

The Mn LDOS presents similar features, with a sharper peak in the case of Mn adsorption on A sites. Since the magnetic moment is an integrated quantity, the differences in magnitudes in B, C, and AA sites are minor. The atomic character of the Mn magnetic moment is still clearly identified (half-filled d orbitals below E_F). In particular the A site yields more localized Mn d states.

The DOS around the Fermi level has few states, but an examination of the orbital contributions shows that it is populated mainly by s electrons. The magnetic moment of the Mn atom has a small contribution from the s electrons, $\sim$10%, 5%, and 3% (for Cu, Ag, and Au, respectively). The only exception is site A, in which the monocoordination and covalent-like bonding produces a higher magnetic moment, which on the gold substrate reaches $5.07\mu_B$. Furthermore, it is worth noticing that in the AA case the interaction of the Mn atom with four atoms (two nearest-neighbor surface atoms and two next-nearest neighbors located at the same layer) produces a local density of states with features similar to the C and B cases, but with smaller peaks.

V. Mn DIMER ADSORPTION

To understand the adatom-substrate interaction, we recalculated the free Mn dimer electronic, magnetic, and structural properties using the method and approximations mentioned here. We obtained the result that in the ground state the two atoms are coupled antiferromagnetically (AFM), with a binding energy per atom of -0.53 eV and a bond length of

2.60 Å. The ferromagnetically (FM) ordered dimer, with the same bond length, has a weaker binding energy of −0.28 eV. These values are close to those from previous calculations,[13] which yield −0.391 eV for the binding energy and a bond length of 2.89 Å. As mentioned above, it is important to stress that the distance between the two Mn atoms determines the magnetic configuration with the lowest energy.

We consider now the adsorption of a second Mn atom in two different situations: one in which the dimer is adsorbed vertically to the surface layer, and other where the two atoms are chemisorbed on neighboring surface sites. Thus, the adsorption of a second Mn atom adds more degrees of freedom and offers a larger set of chemisorption possibilities. In addition to the bond dimer orientation with respect to the noble metal surface, and the type of sites on which they are adsorbed, one must consider different orientations of the magnetic moments of both manganese atoms.

Since the chemisorption energy of a single Mn atom is about four times larger than the binding energy of the free Mn dimer, the electronic properties of the two Mn atoms, once deposited on the surface, are ruled by the Mn-surface interaction. Thus, to find the lowest-energy state one must carry a completely unrestricted calculation to optimize all the parameters of the different geometrical and magnetic configurations.

The most stable adsorption geometries for Mn_2 on the (111) fcc surface of noble metals are shown in Fig. 5. Based on our results for single-atom adsorption, which showed that the B, C, and AA sites are the most stable, we locate in one of those sites the first Mn atom. Then, we optimize all possible configurations with the second Mn atom over B, C, and AA sites or on top the first Mn. In this figure we show the seven different geometrical configurations that are stable on the noble metal surfaces.

In geometries I and III the two Mn atoms occupy A and B neighbor sites. In the first case, the two Mn atoms are chemisorbed in neighbor triangles sharing an apex, and in the second case the triangles share an edge. On the other hand, in geometry II the two Mn atoms are located in equivalent sites A or B. The case in which one Mn atom is on an AA site and the other on a C or B site is denoted as geometry IV. Geometries V and VI correspond to the case in which both Mn atoms are chemisorbed in bridge sites. Finally, configuration VII corresponds to the vertical adsorption on a threefold coordinated surface site.

It is important to notice that the equilibrium distances between the Mn atoms depend on the metal substrate and on the particular geometries. We show also in Fig. 5 the equilibrium Mn_2 bond length and in brackets the ideal distance as defined by the substrate sites. To find the equilibrium configuration, the Mn atoms are located at those ideal distances above the chemisorption sites and then allowed to relax until the minimum energy is obtained.

In the upper, middle, and lower rows of Fig. 5, we show, from left to right, the most stable configurations of the Mn_2 chemisorbed on Cu, Ag, and Au surfaces, respectively. The absorption energy, the magnetic moment, the Mn dimer bond length, and the distance between the Mn atoms and the surfaces for all the cases are given in Table III. Here, we distinguish between the ferromagnetic (FM) and antiferromagnetic (AFM) orientation of the Mn atomic moments.

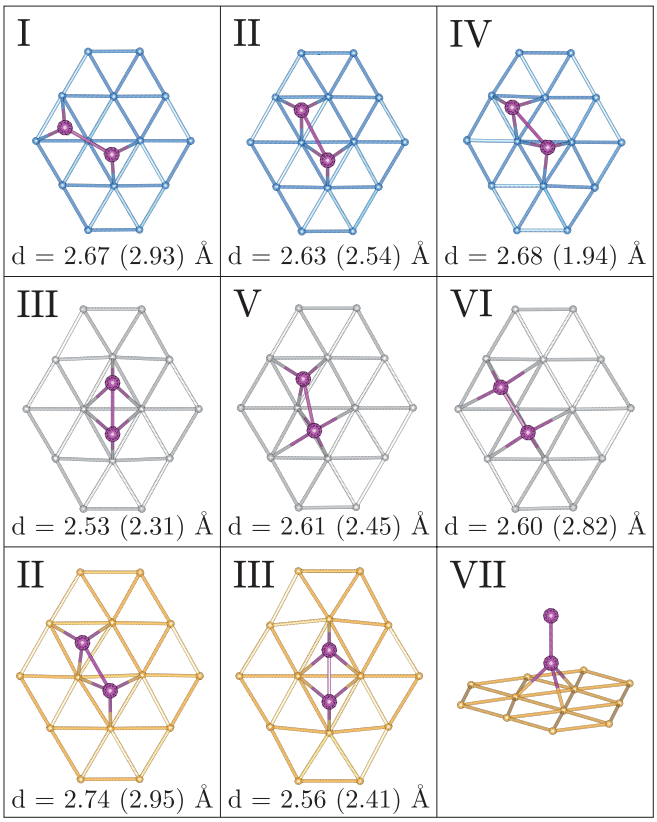

FIG. 5. (Color online) Some geometries on which the Mn_2 is chemisorbed on noble metal (111) surfaces. The upper, middle, and lower panels show the stable geometrical configurations for Cu, Ag, and Au substrates. The figures from left to right correspond to decreasing binding energy configurations. In cases I, II, and III, the dimer is chemisorbed parallel to the surface, on nonequivalent (I, III), and equivalent (II) triangles. In geometry IV, one Mn atom is in a bridge site and the other is in the center of a triangle. In cases V and VI, both Mn atoms are on bridge sites. Case VII corresponds to the dimer chemisorbed, perpendicular to the surface, on a threefold coordinated surface site. In the lower part we give the equilibrium chemisorbed Mn bond length and in brackets we include the distance between chemisorption sites as defined by the surface.

We observe some general trends for the three substrates. (i) The state with smallest binding energy corresponds to geometry VII, the case in which the largest Mn magnetic moment is obtained. This is produced by the single Mn coordination to the surface. (ii) At the equilibrium geometries, the antiferromagnetic state has a stronger binding energy than the ferromagnetic arrangement. (iii) The dimer bond length of the AFM state is smaller than the one with FM coupling.

We now analyze the results for each particular metal. For the Cu substrate we obtain five stable configurations. The one with the strongest binding energy is the one denoted by I in the AFM state (−5.12 eV). We observe that in this case the two Mn atoms occupy sites of type A and B located in neighbor triangles that share an apex. The distance between the two triangle central sites is 2.93 Å but the equilibrium Mn bond length is 2.67 Å, i.e., the two Mn atoms are displaced from the centers toward the Cu atom in between. Configuration II is obtained when we placed both atoms over equivalent A or B sites: the distance between the centers of the triangles is 2.54 Å

TABLE III. Mn_2 adsorption on (111) noble metal surfaces: the adsorption energy is in eV, the magnetic moment is in μ_B, the Mn-Mn bond length ($d_{\text{Mn-Mn}}$), and the Mn-surface ($d_{\text{Mn-surf}}$) distances are given in Å.

	E_A		μ		$d_{\text{Mn-Mn}}$		$d_{\text{Mn-surf}}$	
Site	FM	AFM	FM	AFM	FM	AFM	FM	AFM
Cu I	−5.06	−5.12	8.98	0.00	2.83	2.67	2.49	2.49
Cu II	−5.05	−5.11	8.96	0.00	2.74	2.63	2.41	2.41
Cu III	−4.99	−5.05	8.92	0.00	2.67	2.54	2.37	2.37
Cu IV	−5.08	−5.08	8.97	0.00	2.79	2.68	2.46	2.44
Cu VII	−3.58	−3.59	9.31	0.33	2.67	2.48	2.51	2.49
Ag III	−4.25	−4.27	9.11	0.00	2.63	2.53	2.61	2.59
Ag IV	−4.24	−4.26	9.13	0.02	2.69	2.61	2.70	2.70
Ag V	−4.23	−4.27	9.10	0.05	2.68	2.61	2.66	2.66
Ag VI	−4.25	−4.27	9.07	0.00	2.68	2.60	2.66	2.67
Ag VII	−2.89	−3.07	9.34	0.14	2.66	2.50	2.72	2.69
Au II	−5.45	−5.51	9.28	0.00	2.84	2.74	2.60	2.59
Au III	−5.35	−5.40	9.22	0.00	2.67	2.56	2.52	2.53
Au VII	−3.67	−3.93	9.45	0.25	2.71	2.48	2.61	2.59

but the equilibrium is reached for a bond length of 2.63. To obtain configuration IV, we placed the two atoms in bridge sites, but only one of them remains in that site and the other moves to a threefold coordinated site. The distance between the bridge and central sites is 1.94 Å. The equilibrium Mn bond length is 2.68 Å, i.e., the atoms are strongly displaced, since the distance between chemisorption sites is too small. The chemisorption energy is very similar in these geometries. Comparing the chemisorption energies for the monomer and dimer, we conclude that the latter is more stable and will not dissociate.

In the case of the Ag surface, the energies associated with geometries III, IV, V, and VI are almost equal. This means that the Mn dimer may move very easily along the surface. The bond length differs also very slightly for those cases, and takes a value similar to the one of the free dimer. It is also important to notice that in these cases the FM and AFM solutions differ by only 0.02 eV, and may be present also at finite temperatures. Furthermore, the chemisorption energies on this metal are the smallest among the three noble metals. Similar to the case of Cu, the dimer will not fragment into two monomers.

We find that, in the chemisorption of the Mn dimer on a gold surface, the cases that involve one or both of the Mn atoms on AA bridge sites are unstable; i.e., when the second Mn atom was put over a bridge site, both diffused toward B or C sites. The two stable geometries for the Mn bond lying parallel to the surface are II and III. As mentioned above, the AFM arrangement binds more strongly. The equilibrium bond lengths for the two cases are 2.74 (II) and 2.56 Å(III). Compared with the distances between the centers of the triangles 2.95 (II) and 2.41 (III), we notice a strong modification with respect to the relaxed Mn dimer. Among the three noble metal surfaces, gold most strongly chemisorbes the Mn atoms. Finally, we show in geometry VII the chemisorption of the dimer perpendicular to the surface. In contrast, in Au the Mn dimer will dissociate into two monomers, while it remains for the cases of Cu and Ag.

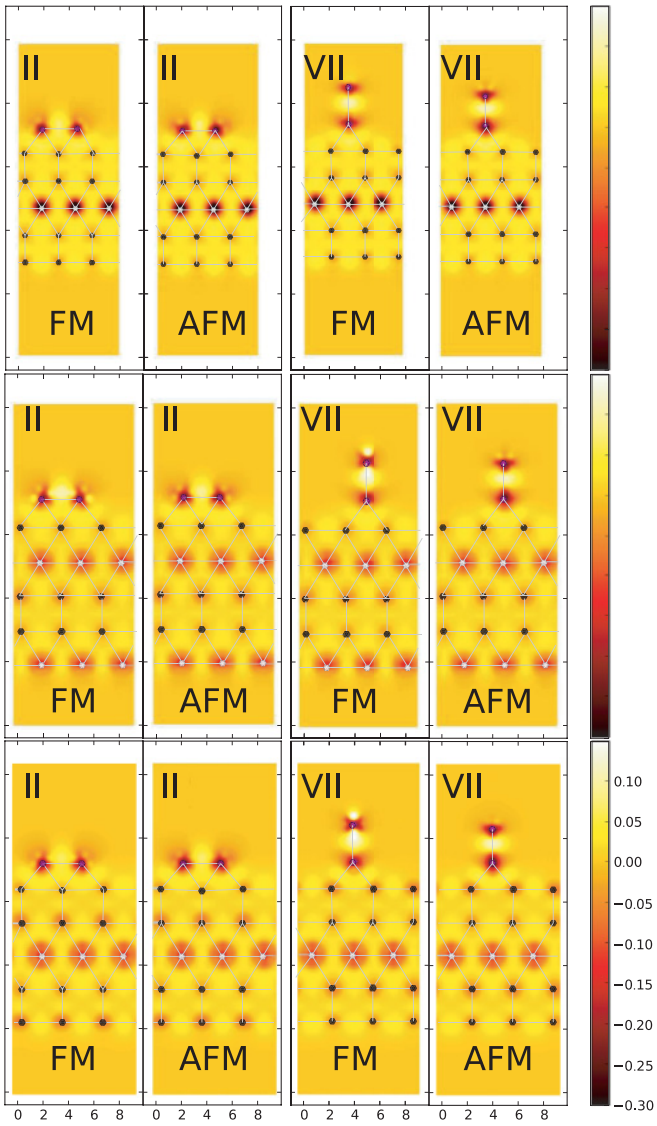

FIG. 6. (Color online) Charge redistribution of Mn_2 adsorbed on (111) noble metal surfaces. The substrate is Cu, Ag, and Au in the upper, middle, and lower panels. The II and VII geometries were calculated assuming ferromagnetic and antiferromagnetic ordering. The scale denotes the distance in Å and the color bars are in units of $e/\text{Å}^3$.

The electronic redistribution after adsorption, for geometries II and VII, is shown in Fig. 6. The upper, middle, and lower panels correspond to Cu, Ag, and Au. The two left panels contain the results for geometry II assuming ferromagnetic and antiferromagnetic coupling. In this case the differences between the two magnetic orientations are small. Nevertheless, it is interesting to note that there is a more intense electronic cloud between the Mn atoms in the case of the Ag substrate. This is in accordance with the longer Mn-Mn bond length of the dimer in Ag and the weakest chemisorption energy.

One observes that in geometry VII there is large deformation of the electronic cloud in the upper Mn atom, which arises from sharing its valence s electron with the lower Mn atom. In contrast with case II, there is a significant difference between

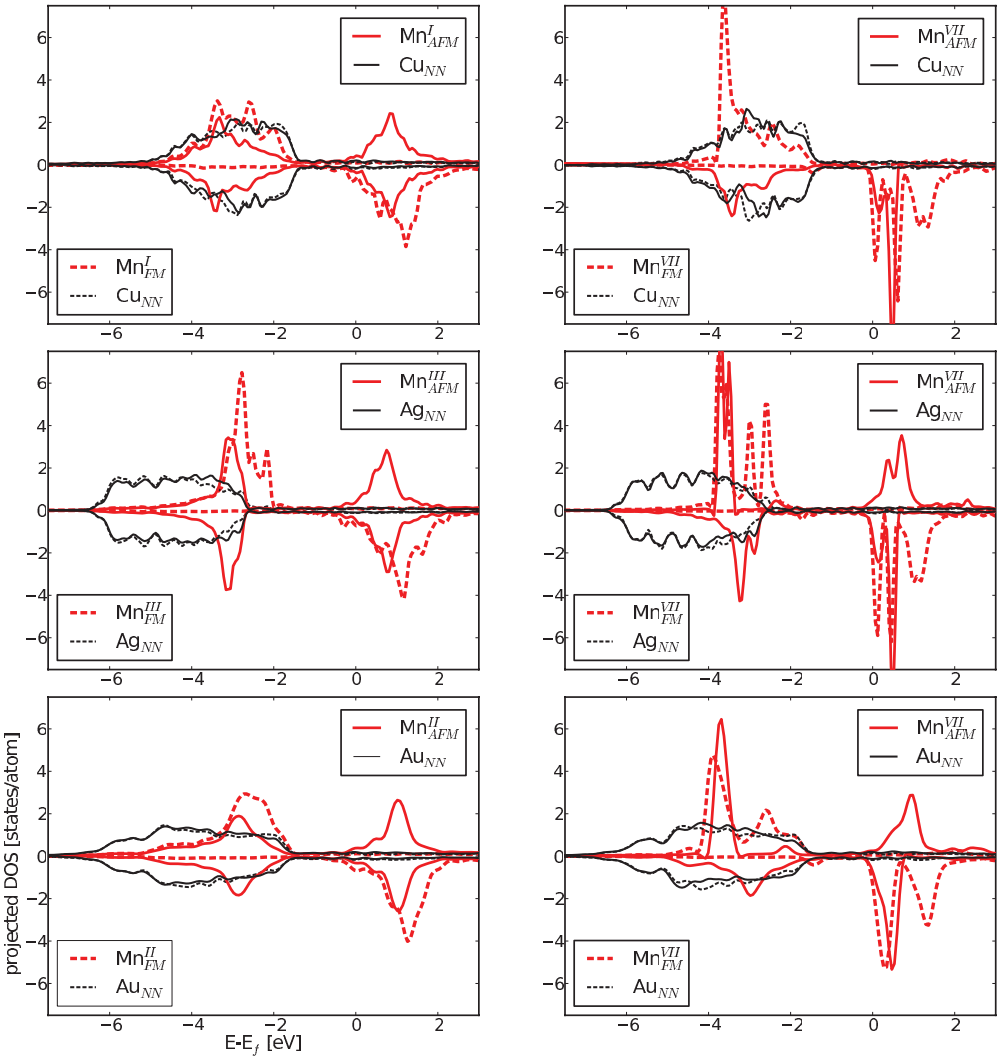

FIG. 7. (Color online) The average local electronic density of states, for spin-up and spin-down electrons, of Mn_2 on noble metal (111) surfaces. The average local densities of states of the surface nearest neighbors are also plotted. The Mn superscript (in the legends) indicates the adsorption geometry of the Mn_2, and the subscript indicates the magnetic order considered. The upper, middle, and lower rows correspond to Cu, Ag, and Au substrates, respectively.

FM and AFM states. One clearly sees the shorter bond in the AFM state.

We present the average electronic local density of states (LDOS) of the chemisorbed dimer in Fig. 7. Here, we show the LDOS for the FM (solid curve) and AFM (broken curve) configurations. In each panel we display the LDOS for spin-up electrons in the upper part and the corresponding spin-down electrons in the lower part. The average LDOS corresponding to the surface nearest neighbors of the Mn atoms are also included (the VII geometry corresponds to the vertical atom perpendicular to the surface and a three-fold coordinated site). The upper, middle, and lower sets of panels correspond to Cu, Ag, and Au, respectively. The Fermi energy is the zero of the energy scale.

One can notice that the *d* bandwidths corresponding to Cu and Ag are of about the same magnitude, but the Ag *d* states have lower energy with respect to the Fermi level. On the other hand the Au *d* bandwidth is the largest of the three metals, and its *d* states are as close to the Fermi energy as the ones of Cu.

In geometry VII, where the Mn dimer is deposited perpendicular to the surface, the LDOS shows large peaks around the bonding and antibonding states of the free dimer. The larger dispersion corresponds to that of Au and Cu. In Ag some of the Mn *d* states fall at the upper border of the *d* band and interact mainly with the *s* band. Furthermore, one observes that, due to the different symmetries of the two Mn atoms, the magnetic moments are of different magnitude. This produces a finite sum of both magnetic moments in the antiferromagnetic solution.

We see that the changes on the electronic structure of the noble metal nearest neighbors are small; only negligible changes around the Fermi energy in the *s* states are observed. This effect produces also very small magnetic moments.

In geometries II and III (also IV and VI, not shown here), where the dimer lies parallel to the surface, the orbital hybridization with a larger number of noble metal atoms produces a more intense electronic dispersion. The bonding and antibonding peaks observed in case VII are smoothed.

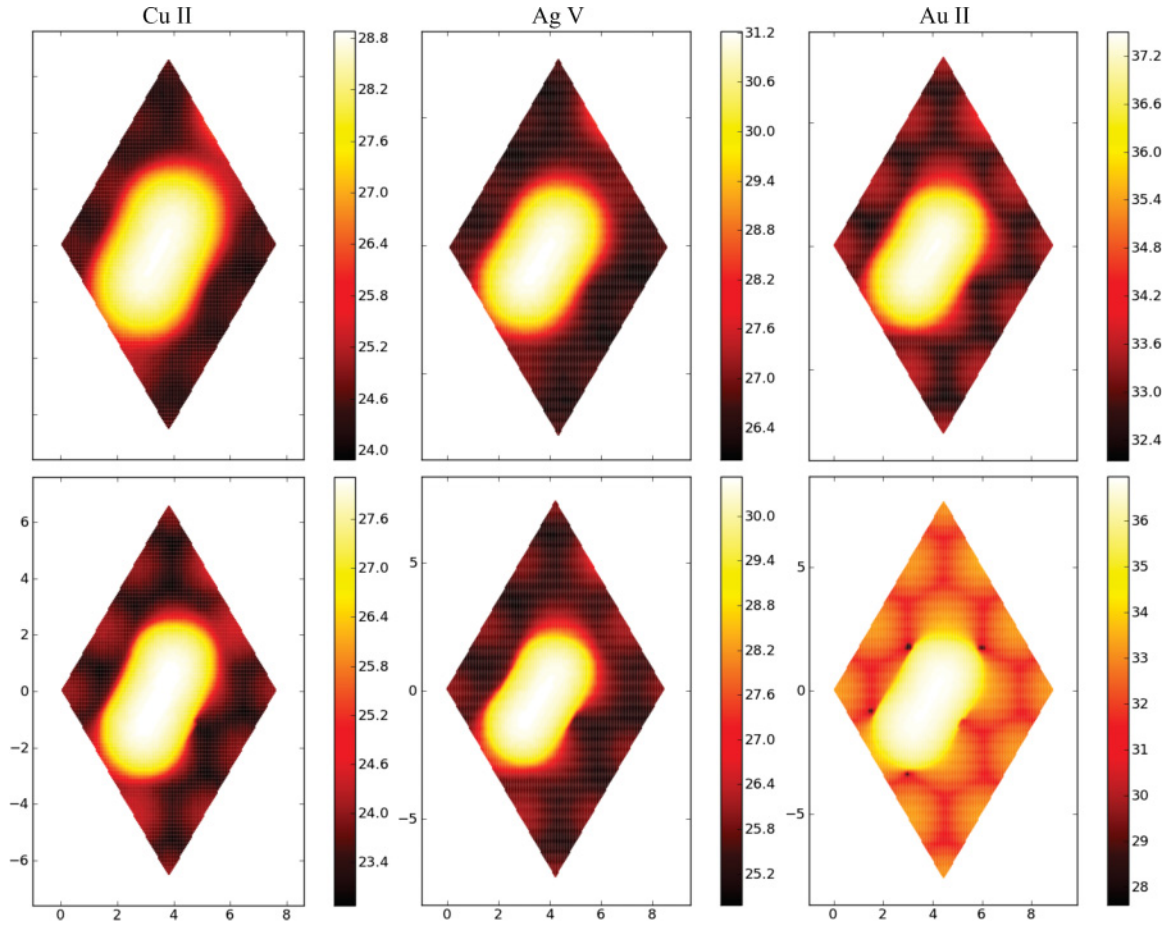

FIG. 8. (Color online) Simulated scanning tunneling microscopy (STM) images for a Mn dimer chemisorbed on a probable geometry on a (111) noble metal surface: II for Cu, and Au, and V for Ag. The applied voltage is 2.0 V and the charge density is kept constant at the values 0.01 (upper) and 0.02 (lower) $e/\text{Å}^3$, respectively. The color bars indicate the depth in Å.

Furthermore, the Mn atoms coordinated to three substrate atoms are symmetric and yield a zero magnetic moment in the AFM configuration. It is interesting to note that, in the FM solution for the Ag substrate, there is a strong interaction between the manganese *d* states and the silver *s* states.

Finally, we calculated scanning tunneling microscopy (STM) images of the stable Mn dimer chemisorption geometries: II for Cu and Au, and V for Ag (see Fig. 5). In Fig. 8 we present the simulations in which the applied voltage was set to 2.0 V, and the upper and lower panels correspond to electronic densities of 0.01 and 0.02 $e/\text{Å}^3$, respectively. With the electronic structure obtained in our calculation, we can extract some topographical information about the Mn dimer and the substrate atoms. In the upper figure one can see mainly the details of the Mn atoms. On the other hand, in the lower figure one can distinguish the surface atoms (light brown in Cu and Ag and yellow in Au). These images may be of interest to experimentalists studying Mn atoms chemisorbed on noble metal surfaces. However, it is important to note that it is difficult to derive the local electronic density of states from STM voltage-current measurements. The results are determined by the applied voltage; the higher that value, the deeper in energy, from the Fermi level, are the electrons sampled in the current.[45,46]

VI. DIFFUSION ENERGY BARRIERS

In addition to the capacity of STM to reveal the topographical conditions of clean and covered surfaces at the atomic level, it has been shown that with the microscope tip one can move chemisorbed atoms and molecules along the surface to form dimers and bigger clusters. This technique has been used to study the electronic structures of Au, Mn, Fe, and Co dimers, and Au linear chains on NiAl (100).[47–49] It has been also reported that one can manipulate single Mn atoms adsorbed on Ag(111) to build clusters up to tetramers.[50]

Thus, it is important to calculate the diffusion energy barriers that the Mn atoms may find if one moves them from the equilibrium positions. To study the dynamics of a Mn dimer over a noble metal surface, we employed the nudge elastic band method as implemented in the VASP package. This method requires the geometrical optimization of several images under a reaction path joined by elastic strings. To perform a large enough number of calculations, we decreased the *K*-point grid to $7 \times 7 \times 1$ by keeping the same energy cutoff. Furthermore, since the Mn_2 AFM state is more stable than the FM alignment, we considered only the Mn atoms oriented antiferromagnetically.

The procedure to study possible diffusive processes is the following: We start from the configuration of minimum energy,

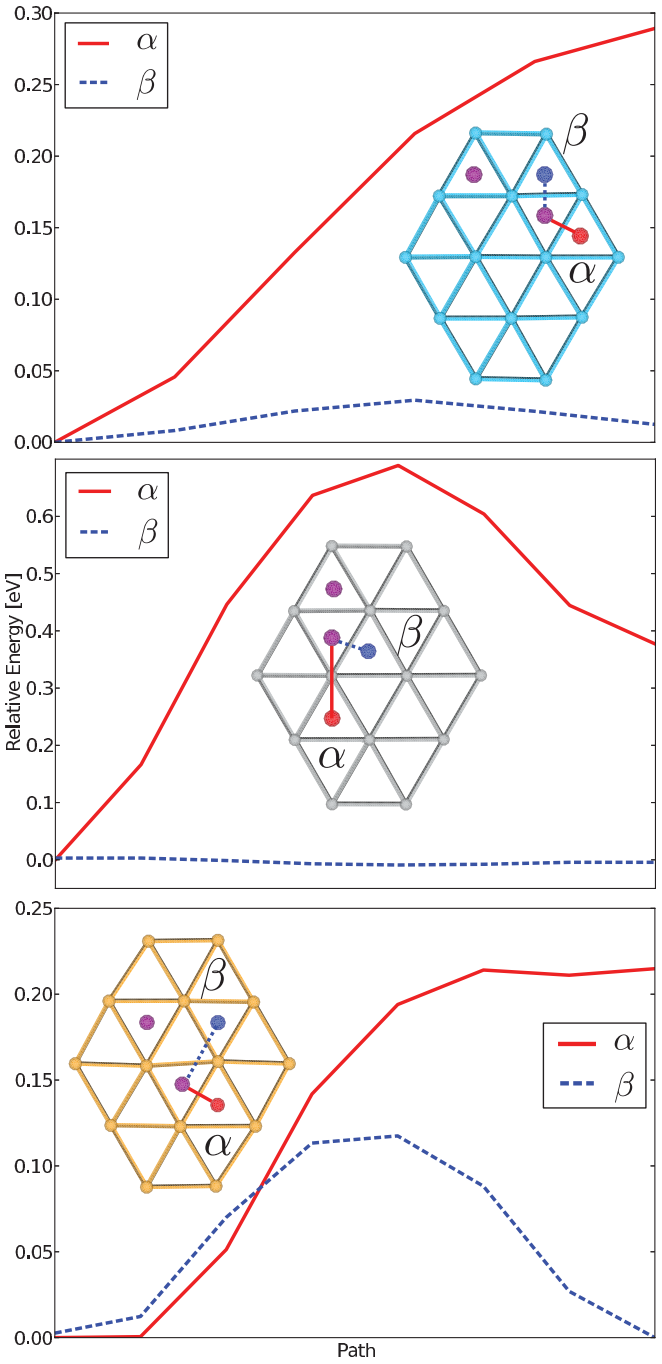

FIG. 9. (Color online) Diffusion of Mn_2 over Cu (upper), Ag (middle), and Au (lower) surfaces. Two paths were studied: dissociation (α, red solid line) and nondissociation (β, blue dashed line) of the Mn dimer. The initial image (purple Mn atoms) corresponds to the minimum energy configurations, I (Cu), III (Ag), and II (Au). One Mn atom is displaced along the vectors while the other remains near its equilibrium site. Note that the energy scale is different in each system.

reported in the previous section. Then, we move one of the two Mn atoms to one of the other threefold coordinated sites. We analyzed two diffusive paths: one that leads to a dissociation of the two Mn atoms, and the second in which the dimer character is preserved but the second atom occupies a neighbor threefold site with different symmetry (B or C). In Fig. 9 we sketch the two paths followed in each of the noble metal surfaces. The first image corresponds to the lowest-energy configuration that we found. One of the final images is obtained following the path called α, by keeping one Mn atom in its original position while the other is translated to a more distant adsorption site; this corresponds to dimer dissociation or a less-bounded dimer. In the second trajectory, marked as β, the last image is calculated by keeping one Mn atom in its original position while the other is moved to another nonequivalent (Cu, Ag) or equivalent (Au) low-energy adsorption site. Between the first and last images, we optimized six intermediate images without imposing any constraint other than the spring forces due the nugde elastic band method. Additionally it is worth noting that in Fig. 9 we show only a representative portion of the supercell.

In general, the dissociation process is energetically unfavorable, with large energy barriers >0.2 eV. The largest value (0.6 eV) was obtained in a Ag surface, since in the diffusion path a Mn atom passes over an A site (such sites are less favorable for chemisorption). Once the barrier is passed, the final configuration has an energy ∼0.4 eV above the original dimer arrangement. Over the Cu surface the Mn_2 dissociation is not possible, at least as far as in our approximation is concerned. This can be partly attributed to the small Cu lattice parameter. Over gold the dissociation barrier is smaller, although it remains large (∼0.2 eV).

The nondissociative paths of diffusion are very interesting. In the Cu surface there is a small energy barrier, ∼0.03 eV, an order of magnitude smaller than in the dissociation path, that can be surpassed by thermal excitations at room temperature. The end point is at slightly higher energy than the starting point. In the case of Ag, there is no energy barrier at all: the curve is completely flat (up to our error bars, estimated up to 0.01–0.02 eV). Therefore the dimer can roam over the surface almost freely (just avoiding the A sites). This behavior explains the fact that the lowest-energy geometries are degenerate. Finally, in gold there is a much larger energy barrier, ∼0.1 eV, which can be hardly overcome at room temperature. This large barrier is expected since the bridge AA site is higher in energy in gold than in Cu and Ag. Also it is interesting to note that in gold the surface atoms rearrange to a larger extent than in Cu and Ag.

VII. SUMMARY AND CONCLUSIONS

We reported an exhaustive set of calculations of the monoatomic and dimer adsorption of manganese on (111) noble metal surfaces, performed within the DFT as implemented in the VASP code. To visualize the electronic charge distribution, we plotted the difference between the converged charge density of the system under study and the superposition of atomic charge densities. We also reported the spin-dependent electronic local densities of states for some of the calculated geometries.

In order to study the effects produced by the Mn adsorption and to prove the validity of our approximations, we calculated first the free noble metal surface characteristics. The experimentally observed contraction of the first surface layer in Cu and Ag, and the expansion in Au, were acceptably reproduced. Then, we modeled the chemisorption of one Mn atom on

four surface sites with different geometries and symmetries. We calculated the chemisorption binding energy and found that, among the three metals, Au binds the Mn atom the most strongly, and Ag the most weakly. The most stable geometry corresponds to the adsorption on the threefold coordinated hollow sites. The calculated magnetic moments of the Mn atom chemisorbed at those sites are $4.53\mu_B$, $4.77\mu_B$, and $4.83\mu_B$ on Cu, Ag, and Au, respectively.

To study the dimer adsorption, we calculated with the same method the free dimer properties. Then we located the dimer perpendicular and parallel to the surface. We found that the most favorable geometry corresponds to the dimer lying parallel to the surface with its atoms occupying three coordinated hollow sites. The equilibrium bond lengths of the most stable configurations are 2.67, 2.53, and 2.74 Å, with chemisorption energies of −5.12, −4.27, and −5.51 eV for Cu, Au, and Au, respectively. The values for the free dimer are 2.60 Å, and −0.53 eV. Comparing the binding energies to the monomer adsorption, one concludes that the dimer breaks into monomers only in the case of Au.

In all cases, the Mn antiferromagnetic configuration is more stable than the ferromagnetic alignment. Compared to the monomer case, the stronger hybridization with the surface atoms reduces the value of the Mn atomic magnetic moment to about $4.6\mu_B$ per atom.

It is important to note that, in the case of Ag, three different geometries have similar chemisorption energy (cases III, V, and VI). This result may indicate that the dimer may move very easily along the surface. Another important result for this substrate is that the ferromagnetic solutions are close in energy to the antiferromagnetic most-stable state. Thus, one can expect that this arrangement may be also present at finite temperatures.

We calculated the energy barriers for Mn diffusion along the surface. These results may be of interest to experimentalists using the tunneling tip in STM to move chemisorbed atoms along the surface. Finally, we calculated scanning tunneling microscopy images of the most stable configurations of the Mn dimer on the noble metal substrates. One can clearly see the topography of the Mn dimer and the surface atoms. Investigations of the chemisorption of larger Mn clusters are in progress.

ACKNOWLEDGMENTS

The authors thanks the support from FONDECYT through Grants No. 1100365 (J.M.-L.) and No. 11110510 (F.M.), from Grant ICM P10-061-F by Fondo de Innovación para la Competitividad-MINECON, from Financiamiento Basal para Centros Científicos y Tecnológicos de Excelencia, under Project No. FB 0807, and from CONACYT (México) through Grants No. 61417 and No. J-152153-F. The use of computer resources from the Centro Nacional de Supercómputo (CNS) of the Instituto Potosino de Investigación Científica y Tecnológica (IPICYT), SLP, México and the TACC Supercomputer center in Texas are also acknowledged.

[1] C. Binns, Surf. Sci. Rep. **44**, 1 (2001).
[2] B. Belhadji, S. Lounis, M. Benakki, and C. Demangeat, Phys. Rev. B **69**, 064431 (2004).
[3] G. Bihlmayer, P. Kurz, and S. Blügel, Phys. Rev. B **62**, 4726 (2000).
[4] C. Biswas, R. S. Dhaka, A. K. Shukla, and S. R. Barman, Surf. Sci. **601**, 609 (2007).
[5] M. Hortamani, H. Wu, P. Kratzer, and M. Scheffler, Phys. Rev. B **74**, 205305 (2006).
[6] P. Krüger, M. Taguchi, and S. Meza-Aguilar, Phys. Rev. B **61**, 15277 (2000).
[7] O. Rader, T. Mizokawa, A. Fujimori, and A. Kimura, Phys. Rev. B **64**, 165414 (2001).
[8] V. S. Stepanyuk, L. Niebergall, R. C. Longo, W. Hergert, and P. Bruno, Phys. Rev. B **70**, 075414 (2004).
[9] E. Simon, B. Újfalussy, B. Lazarovits, A. Szilva, L. Szunyogh, and G. M. Stocks, Phys. Rev. B **83**, 224416 (2011).
[10] C. Demangeat and J. C. Parlebas, Rep. Prog. Phys. **65**, 1679 (2002).
[11] D. Hobbs, J. Hafner, and D. Spišák, Phys. Rev. B **68**, 014407 (2003).
[12] M. B. Knickelbein, Phys. Rev. Lett. **86**, 5255 (2001).
[13] J. Mejía-López, A. H. Romero, M. E. Garcia, and J. L. Morán-López, Phys. Rev. B **74**, 140405 (2006).
[14] J. Mejía-López, A. H. Romero, M. E. Garcia, and J. L. Morán-López, Phys. Rev. B **78**, 134405 (2008).
[15] B. T. Jonker, J. J. Krebs, and G. A. Prinz, Phys. Rev. B **39**, 1399 (1989).
[16] O. Rader, W. Gudat, C. Carbone, E. Vescovo, S. Blügel, R. Klässges, W. Eberhardt, M. Wuttig, J. Redinger, and F. J. Himpsel, Phys. Rev. B **55**, 5404 (1997).
[17] C. Ross, B. Schirmer, M. Wuttig, Y. Gauthier, G. Bihlmayer, and S. Blügel, Phys. Rev. B **57**, 2607 (1998).
[18] P. Schieffer, C. Krembel, M. C. Hanf, G. Gewinner, and Y. Gauthier, Phys. Rev. B **62**, 2944 (2000).
[19] M. Fonin, Y. Dedkov, U. Rüdiger, and G. Güntherodt, Surf. Sci. **529**, L275 (2003).
[20] M. Wuttig, Y. Gauthier, and S. Blügel, Phys. Rev. Lett. **70**, 3619 (1993).
[21] Y. Huttel, C. M. Teodorescu, F. Bertran, and G. Krill, Phys. Rev. B **64**, 094405 (2001).
[22] U. Manju, D. Topwal, G. Rossi, and I. Vobornik, Phys. Rev. B **82**, 035442 (2010).
[23] S. Uzdin, V. Uzdin, and C. Demangeat, Surf. Sci. **482**, 965 (2001).
[24] M. Kabir, D. G. Kanhere, and A. Mookerjee, Phys. Rev. B **75**, 214433 (2007).
[25] S. Uzdin, V. Uzdin, and C. Demangeat, Europhys. Lett. **47**, 556 (1999).
[26] V. S. Stepanyuk, W. Hergert, K. Wildberger, S. K. Nayak, and P. Jena, Surf. Sci. **384**, L892 (1997).
[27] F. Muñoz, A. H. Romero, J. Mejía-López, and J. L. Morán-López, Phys. Rev. B **83**, 205423 (2011).
[28] S. Mathias, M. Wiesenmayer, M. Aeschlimann, and M. Bauer, Phys. Rev. Lett. **97**, 236809 (2006).
[29] T. Chiang, AAPPS Bull. **18**, 2 (2008).
[30] R. Martin, *Electronic Structure: Basic Theory and Practical Methods* (Cambridge University Press, Cambridge, UK, 2004).
[31] G. Kresse and J. Hafner, Phys. Rev. B **47**, 558 (1993).

[32]G. Kresse and J. Hafner, Phys. Rev. B **49**, 14251 (1994).
[33]G. Kresse and J. Furthmüller, J. Comp. Mater. Sci. **6**, 15 (1996).
[34]G. Kresse and J. Furthmüller, Phys. Rev. B **54**, 11169 (1996).
[35]P. E. Blöchl, Phys. Rev. B **50**, 17953 (1994).
[36]G. Kresse and D. Joubert, Phys. Rev. B **59**, 1758 (1999).
[37]J. P. Perdew, K. Burke, and M. Ernzerhof, Phys. Rev. Lett. **77**, 3865 (1996).
[38][http://www.webelements.com].
[39]S. Å. Lindgren, L. Walldén, J. Rundgren, and P. Westrin, Phys. Rev. B **29**, 576 (1984).
[40]P. Statiris, H. C. Lu, and T. Gustafsson, Phys. Rev. Lett. **72**, 3574 (1994).
[41]A. R. Sandy, S. G. J. Mochrie, D. M. Zehner, K. G. Huang, and D. Gibbs, Phys. Rev. B **43**, 4667 (1991).
[42]J. Wan, Y. L. Fan, D. W. Gong, S. G. Shen, and X. Q. Fan, Modelling Simul. Mater. Sci. Eng. **7**, 189 (1999).
[43]S. M. Foiles, M. I. Baskes, and M. S. Daw, Phys. Rev. B **33**, 7983 (1986).
[44]Y. Wang, N. S. Hush, and J. R. Reimers, Phys. Rev. B **75**, 233416 (2007).
[45]J. Li, W.-D. Schneider, and R. Berndt, Phys. Rev. B **56**, 7656 (1997).
[46]M. Becker and R. Berndt, Phys. Rev. B **81**, 035426 (2010).
[47]N. Nilius, T. M. Wallis, M. Persson, and W. Ho, Phys. Rev. Lett. **90**, 196103 (2003).
[48]H. J. Lee, W. Ho, and M. Persson, Phys. Rev. Lett. **92**, 186802 (2004).
[49]T. M. Wallis, N. Nilius, and W. Ho, Phys. Rev. Lett. **89**, 236802 (2002).
[50]J. Kliewer, R. Berndt, J. Minár, and H. Ebert, Appl. Phys. A **82**, 63 (2006).